PCCP

Accepted Manuscript

ROYAL SOCIETY OF CHEMISTRY

www.rsc.org/pccp

Physical Chemistry Chemical Physics

ARTICLE

Magnetic Two-dimensional Molecularly Imprinted Materials for Recognition and Separation of Proteins

Received

Accepted

DOI:

www.rsc.org/

Fangfang Chen, Weifeng Zhao, Jingjing Zhang and Jie Kong*

Surface molecular imprinting for proteins is an emerging cross field of molecular imprinting engineering and functional materials. In this contribution, we report a novel design of magnetic two-dimensional molecularly imprinted polymers (2D-MIPs) for high recognition and separation of proteins. The bovine serum albumin-surface-imprinted polydopamines were prepared on the surfaces of magnetic Fe_3O_4–graphene oxide hybrid to form magnetic 2D-MIPs for proteins. The 2D Fe_3O_4–graphene oxide substrate possesses a dominant surface-to-volume ratio in comparison to 3D spherical substrate with the same volume. These materials are sensitive to a magnetic field and can be easily separated using an external magnet. The binding experiment results of bovine serum albumin on magnetic 2D-MIPs and real sample analysis demonstrated high recognition specificity, selectivity, accessibility and convenient separation of 2D-MIPs for template protein. The design and synthesis of magnetic 2D-MIPs provide a new perspective for the surface molecularly imprinted materials with potential in recognition and separation of proteins.

Introduction

Proteins, such as antibodies and enzymes are usually employed as recognition elements for diagnosis and disease therapeutics. Therefore, selective recognition and separation of target proteins from complex samples have received numerous attentions. Molecular imprinting is an effective technique to produce specific binding sites in a synthetic polymer matrix, which is complementary in shape, size, and functionality with respect to target template molecules.[1-3] Molecularly imprinted polymers (MIPs) with molecular recognition functionality have been regarded as a promising alternative to enzymes, antibodies, and natural receptors for application in biosensing,[4] bioseparation,[5] medical diagnostics,[6] and drug delivery.[7] Numerous MIPs have been successfully developed for small molecules,[8-10] however, imprinting proteins and biomacromolecules still faces challenge because of the molecular dimension, conformational flexibility, solubility and mass transfer. In this emerging field, several strategies have been adopted for imprinting proteins, including designing functional monomers with good biocompatibility,[11] epitope approach,[12] metal-coordination polymerization,[13] and surface molecular imprinting.[14]

Surface molecular imprinting in which a thin imprinted layer is coated on the surfaces of solid supports is beneficial for the removal and rebinding of the template proteins between polymers and solutions.[15] The supports are typically silica beads,[16] polymer particles,[17] carbon nanotubes,[18] Fe_3O_4 nanoparticles (NPs).[19] Graphene, a single-layer carbon atoms,[20] is one of cutting-edge two-dimensional nanomaterials with extraordinary properties and wide potential in energy, biomaterials and environment. Accordingly, graphene is also an excellent possible candidate of supports for MIPs.[21] In comparison to three-dimensional silica or nanoparticles, the two-dimensional structure of graphene or graphene oxide is prefer to give a dominant surface-to-volume ratio as illustrated in **Scheme 1**. If molecularly imprinted polymers are coated on the surfaces of this two-dimensional structure, a novel molecular imprinting material, named two-dimensional molecular imprinting polymer (2D-MIP), is expected to possess high specificity and selectivity. On the other hand, the binding cavities of the thinner MIPs layers can significantly improve the accessibility and give a convenience to the recognition and separation of protein with large molecular weight. Some previous studies have shown that MIPs on graphene surface provide a high loading capacity and reduce the binding time of template molecules.[22, 23] However, it is difficult to separate the graphene-MIPs from solution by conventional centrifugation and filtration, which has restricted their application. Fe_3O_4 NPs exhibit super paramagnetic and magnetic susceptibility properties, which make magnetic separation with an external magnetic field possible. Because of the advantages of graphene and Fe_3O_4, the Fe_3O_4–graphene composites have been developed in MIP fields.[24] But there are few studies of MIP-based adsorbents for proteins by using Fe_3O_4–graphenes as the substrates.

Dopamine (DA) containing catechol and amine groups can easily form thin, surface-adherent layers by self-polymerization onto supports in a weak alkaline media.[25] The formed polydopamine (PDA) molecular imprinting layers with good biocompatibility and hydrophilicity are especially appropriate for imprinting and

*MOE Key Laboratory of Space Applied Physics and Chemistry, Shaanxi Key Laboratory of Macromolecular Science and Technology, School of Science, Northwestern Polytechnical University, Xi'an, 710072, P.R. China, *E-mail: kongjie@nwpu.edu.cn, Tel.(fax): +86-29-88431621*

recognition proteins.[26-28] As inspired from the 2D-molecular imprinting concept presented above, if the PDA molecular imprinting layers are formed on the surface of Fe_3O_4 NPs-deposited graphenes,[29] the magnetic 2D-MIPs are very fascinating. Obviously, the 2D structure is helpful to enhancing specificity, selectivity and accessibility of proteins and the paramagnetic property is convenient to magnetic separation with an external magnetic field.

	r (nm)		
	25	50	100
S_{2D}/S_{3D}	16.7	33.2	66.7

Scheme 1 The superficial area ratio of two-dimensional substrate to three-dimensional spherical substrate with the same volume, where S_{2D} represents the superficial area of two-dimensional substrate while its thickness is 1 nm. S_{3D} represents the superficial area of spherical substrate while its radius is *r*.

In this contribution, we report a novel design of magnetic 2D-molecularly imprinted materials for high recognition and separation of proteins. Since the DA was a reducing agent for graphene oxide (GO), the bovine serum albumin (BSA)-surface-imprinted PDA were obtained on Fe_3O_4–graphene oxide (Fe_3O_4–GO) via self-polymerization of DA monomers. The binding experiments of BSA on magnetic 2D-MIPs demonstrated high specificity, selectivity, accessibility and convenient separation of template proteins. To the best of our knowledge, the magnetic Fe_3O_4–graphene PDA-based 2D MIPs for proteins have not been reported. It will provide a new perspective for the surface molecularly imprinted materials with potential in recognition and separation of proteins.

Experimental

Materials.

Natural graphite with an average diameter of 30μm was purchased from a graphite company (Qingdao, China).Dopamine hydrochloride (DA), sodium dodecyl sulfate (SDS), $FeCl_3\,6H_2O$ and $FeCl_2\,4H_2O$ were purchased from Aladdin Reagent Co., Ltd. (Shanghai, China). Albumin from bovine serum (BSA), hemoglobin (Hb), and ovalbumin (Ova) were purchased from Sigma–Aldrich (Tokyo, Japan). Ribonuclease A (RNase A) and Lysozyme (Lyz) were supplied by Amresco (Solon, OH, USA). All other chemicals were of analytical grade and were used as received without further purification unless stated otherwise.

Characterization. Fourier Transform Infrared Spectroscopy (FT-IR) was recorded on a Nicolet iSTO spectrometer (Varian, Palo Alto, California, USA) over a range from 4000 cm^{-1} to 400 cm^{-1}. The morphology of the resultant materials was determined by transmission electron microscopy (TEM) using a Tecnai G2 20-S-TWIN microscope. Thermal gravimetric (TGA) analysis was conducted by a STA 449 F3 instrument (Netzsch GmbH & Co., Selb, Germany) with a heating rate of 10 K/min under argon atmosphere (a gas flow of 50 mL/min) in a temperature range between room temperature and 1000 ^oC. X-ray Photoelectron Spectroscopy (XPS) measurement was conducted on a K-Alpha spectrometer (Axis Ultra, Kratos Analytical Ltd., U.K.) and the core level spectra were measured using a monochromatic Al Ka X-ray source (hv=1486.7 eV). The analyzer was operated at 23.5 eV pass energy and the analyzed area was 200-800 μm in diameter. The lowest energy resolution is 0.48 eV (Ag 3d5/2). Binding energy was referenced to the adventitious hydrocarbon C1s line at 285.0 eV. The magnetic properties were measured using an MPMS Squid vibrating sample magnetometer (VSM) (San Diego, USA).The crystal structures were characterized by a Bruker D8 Advance X-ray diffraction (XRD) using Cu Kα radiation (Bremen, Germany). UV-vis spectra were recorded on a Xinmao Ultraviolet–Visible (UV–Vis) spectrophotometer (UV-7504 PC). Real samples were analyzed on Shimadzu LC-20A high performance liquid chromatography-UV system (HPLC-UV) equipped with diode array detector (Kyoto, Japan). The injection volume and detection wavelength were 10 μL and 214 nm, respectively. The analytical column was a 250 mm × 4.6 mm, 5 μm Hypersil 300A-C_8 column (Elite). The mobile phase consisted of 0.1% trifluoroacetic acid water solution (A) and acetonitrile (B) with the flow rate of 1.0 mL min^{-1} for linear gradient elution with solvent B increasing from 30% to 60% in 20 min.

Synthesis of Fe_3O_4-GO. The GO was synthesized from natural graphite according to Hummers method.[30,31] Fe_3O_4–GO was synthesized by co-precipitation between Fe^{2+} and Fe^{3+} in the presence of GO with some modification as described by Thu et al.[32] First, $FeCl_3\,6H_2O$ (271 mg) and $FeCl_2\,4H_2O$ (99.5 mg) were dispersed in 30 mL deionized water under sonication for 10 min. Second, 30 mL GO solution (5 mg/mL) was added and stirred for 30 min at room temperature. Third, 2 mL of ammonia was added dropwise to the mixture under nitrogen, where the solution color was changed to black. This black mixture was vigorously stirred for 30 min at 50 °C. Finally, the black precipitate (Fe_3O_4–GO) was collected from the reaction medium using a magnet and then repeatedly washed with deionized water until the pH of the washing solution became neutral.

Synthesis of BSA-Fe_3O_4/GO/PDA 2D-MIPs. The BSA-Fe_3O_4/GO/PDA 2D-MIPs were synthesized as follows.[21] In a typical synthesis, Fe_3O_4–GO (20 mg) was first dispersed in 20 mL of a phosphate buffer (0.2 mol/L, pH=7.4) under sonication for 10 min. Second, BSA (20 mg) was then added and stirred for 30 min at room temperature. Subsequently, DA (100 mg) was added, and the reaction was continued for 5 h at room temperature. The BSA-Fe_3O_4/GO/PDA 2D-MIPs were collected magnetically, washed with water to remove the unreacted monomer, followed by washing with a 10% w/v SDS solution for removing the template protein and thoroughly rewashing with distilled water. As a comparison, the Fe_3O_4/GO/PDA NIPs (non-imprinted polymers) were prepared using the same method as BSA-Fe_3O_4/GO/PDA 2D-MIPs, albeit without the addition of the template protein.

Adsorption Experiment. In kinetics experiment, 10 mg of Fe_3O_4/GO/PDA 2D-MIPs or NIPs was added to a centrifuge tube containing 5 mL of a BSA solution (1.5 mg/mL) and ultrasonically dispersed for 1 min. The mixture was subjected to shaking for a period of time at room temperature. Next, the samples were withdrawn at appropriate time intervals, and a magnet was deposited at the outside of the tube to separate the Fe_3O_4/GO/PDA 2D-MIPs or NIPs from the solution, and then the supernatant was subjected to UV measurements on a UV-7504 PC spectrophotometer at a detection wavelength of 278 nm.

The adsorption isotherm test was conducted to evaluate the capacity of the prepared materials for recognizing and binding BSA. For this purpose, 10 mg of Fe_3O_4/GO/PDA 2D-MIPs or NIPs was added to a centrifuge tube containing 5 mL of a BSA solution with a certain concentration, and the centrifuge tube was subjected to shaking for 1 h at room temperature. After magnetic separation, the BSA concentration in the supernatant was measured by UV at 278 nm. The adsorption capacities (Q, mg/g) of the Fe_3O_4/GO/PDA 2D-MIPs or NIPs for the template protein were calculated from the differences in the protein concentration before and after adsorption by the following equation (1):

$$Q = (C_0 - C_e)V / m \qquad (1)$$

where C_0 and C_e are the concentrations (mg/mL) of the template in the solution before and after sorption, respectively, V is the volume of BSA solution (mL), and m is the mass of Fe_3O_4/GO/PDA 2D-MIPs or NIPs (g). The selectivity of the magnetic imprinted sorbent was investigated using Hb, Ova, RNase A, and Lyz with initial concentrations of 1 mg/mL. 10 mg of Fe_3O_4/GO/PDA 2D-MIPs or NIPs was added to a centrifuge tube containing 5 mL of protein solution, and the centrifuge tube was subjected to shaking for 10 min at room temperature.The amount of free protein was measured using a UV–Vis spectrophotometer.

Real Sample Analysis. The Fe_3O_4/GO/PDA 2D-MIPs were applied to selectively separate the BSA from a real bovine blood sample. The blood sample was diluted 200-fold with Tris-HCl buffer (10 mM, pH=7.0). The 2D-MIPs or NIPs (20 mg) were incubated with the diluted blood solution (5 mL) for 10 min at room temperature. Then, 0.1 M NaOH was used to elute the adsorbed protein for 2 h. The standard BSA solution, diluted blood sample, and eluted samples from 2D-MIPs or NIPs were injected for the HPLC-UV analysis.

Results and Discussion

Design and Synthesis of Magnetic 2D-MIPs for Proteins. The main object of this work was to present a new design and synthesis of magnetic proteins-imprinted materials with two-dimensional structure. As shown in **Scheme 1**, the two-dimensional substrate possesses a dominant surface-to-volume ratio in comparison to spherical substrate. If it is presumed that the two substrates have the same volume, the superficial area ratio of two-dimensional to spherical substrate can be calculated according to equation (2).

$$S_{2D} / S_{3D} = \frac{2 \times 4\pi r^3 / 3}{4\pi r^2} = 2r / 3 \qquad (2)$$

where S_{2D} represents the superficial area of two-dimensional substrate while its thickness is 1 nm, S_{3D} represents the superficial area of spherical substrate while its radius is r. Normally, the 3D nanoparticles dimension is 50-200 nm, so the maximum superficial ratio of 2D structure to 3D structure is 67. Thus, the 2D structure provides an opportunity for the high specificity, selectivity and accessibility of proteins.

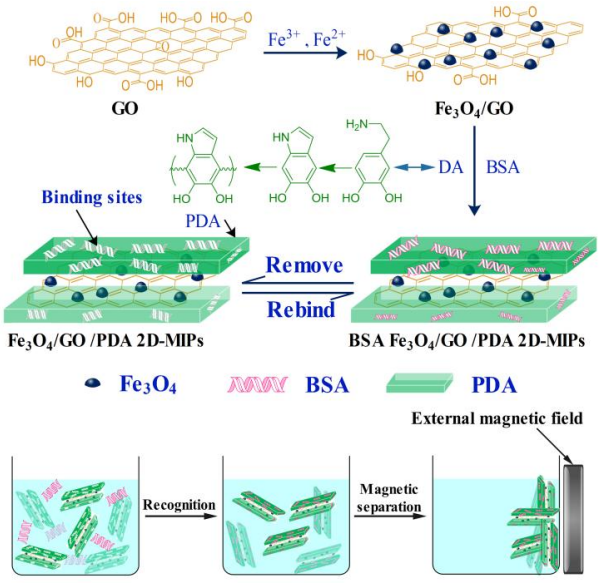

Scheme 2 The schematic illustration of the preparation of Fe_3O_4/GO/PDA two-dimensional molecularly imprinted materials.

Under this guideline, a schematic illustration for preparing magnetic BSA-Fe_3O_4/GO/PDA 2D-MIPs is shown in **Scheme 2**. The TEM images of GO and Fe_3O_4/GO in **Figure 1a** show a typically curved, layer-like structure of GO with a fairly smooth surface. After the iron aqua complexes were mixed and hydrolyzed using an alkaline solution and forming magnetite nuclei, the Fe_3O_4 NPs were consistently deposited onto the GO surface as proved by the TEM observation in **Figure 1b**. Since the DA can be served as a reducing and capping agent for the resulting reduced-GO for stabilization and decoration. When Fe_3O_4–GO was mixed with DA in a BSA-containing solution, the GO were reduced by DA accompanied with the self-polymerization of DA around the resulting GO surface to afford a thin PDA film. At the same time, the template proteins were then embedded in the PDA film. At last, the BSA-Fe_3O_4/GO/PDA 2D-MIPs were obtained after the removal of the embedded BSA template. Further, different amounts of BSA ranged from 5 to 25 mg were investigated to evaluate the influence of BSA amount and the usage of Fe_3O_4–GO and DA were 20 mg and 100 mg, respectively. The results of adsorption experiments were presented in **Table S1**, which showed that the adsorption capacity (Q, mg/g) of BSA on 2D-MIPs increased with increasing BSA content from 5 mg to 20 mg because of the increase in the number of recognition cavities. When the content of BSA is increased at 30 mg, a slight increase in the

adsorption amount could be observed. Therefore, the optimized BSA template content of 20 mg was selected. The structures of Fe_3O_4/GO/PD 2D-MIPs were examined by TEM. As shown in **Figure 1c**, the PDA coating layers are covering the surfaces of 2D Fe_3O_4/GO in comparison to the pure 2D GO and Fe_3O_4/GO structures in **Figure 1a-b**.

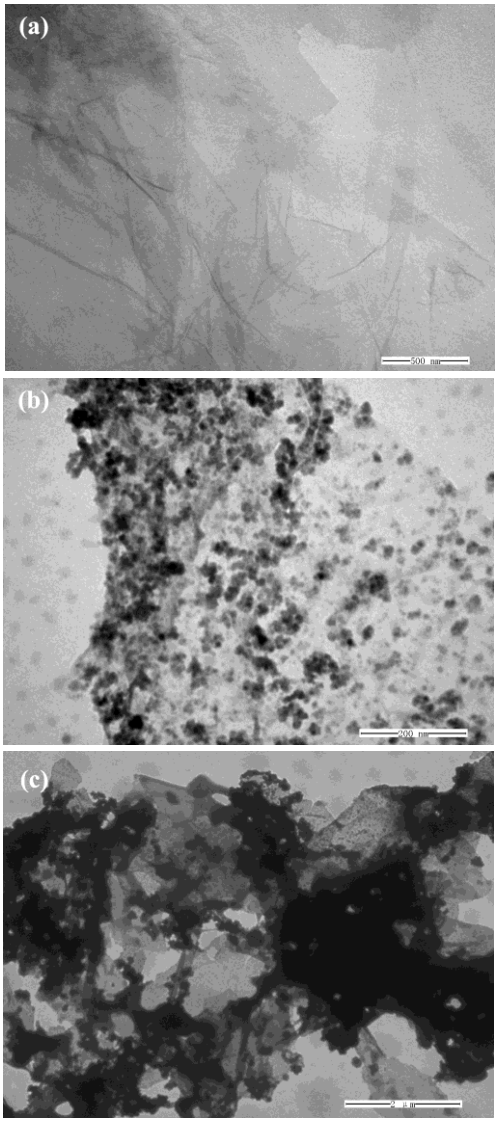

Figure 1 TEM images of GO (a), Fe_3O_4-GO (b) and Fe_3O_4/GO/PDA two-dimensional molecularly imprinted materials (c).

As shown in **Figure 2a**, the FTIR spectrum of GO exhibited strong bands at 3413 cm^{-1} and 1735 cm^{-1}, corresponding to the –OH and C=O groups, respectively. While in the FTIR spectra of Fe_3O_4–GO, the absorption band of Fe_3O_4 was observed at 579 cm^{-1}, suggesting that Fe_3O_4 NPs were embedded on the surface of GO. Compared to the pure GO and Fe_3O_4-GO, Fe_3O_4/GO/PDA 2D-MIPs and NIPs exhibited two absorption peaks at 1646 and 1517 cm^{-1}, corresponding to the phenyl groups. It provides another evidence for the formation of the PDA layers on 2D surfaces. At the same time, the peaks at 1735 cm^{-1} indicates the reduction of the C=O groups of GO.

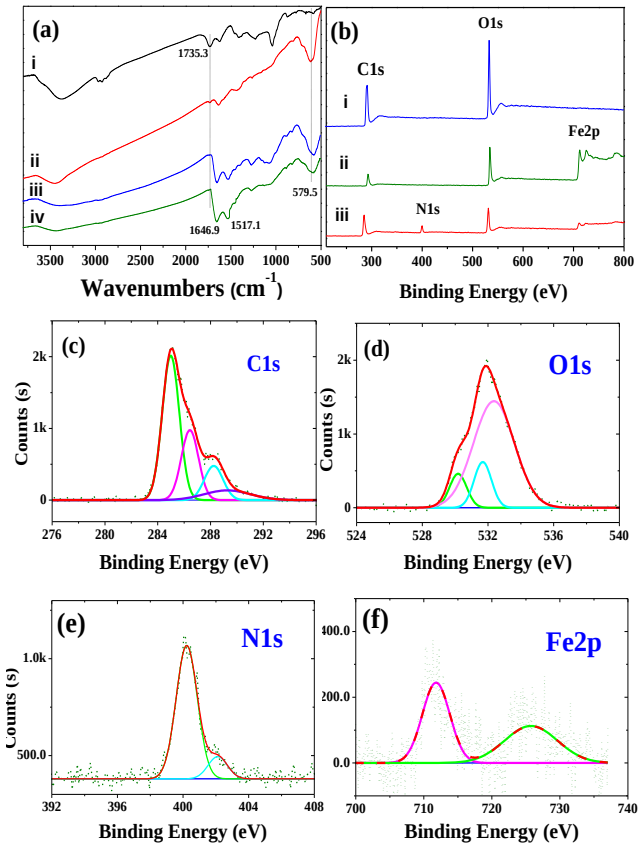

Figure 2 FTIR spectra (a) of GO (i), Fe_3O_4/GO (ii), Fe_3O_4/GO/PDA 2D-MIPs (iii) and Fe_3O_4/GO/PDA 2D-NIPs (iv), XPS spectra (b) of GO (i), Fe_3O_4/GO (ii) and Fe_3O_4/GO/PDA 2D-MIPs (iii), and high-resolution XPS spectra (c-C1s, d-O1s, e-N1s, f-Fe2p) of Fe_3O_4/GO/PDA-MIPs.

For the XPS analysis, **Figure 2b-f** shows the survey and high-resolution spectra of GO, Fe_3O_4–GO, and Fe_3O_4/GO/PDA 2D-MIPs. In general, C1s peak was observed at 285 eV and O1s peak was observed at 527 eV, which was attributed to the surface hydroxyl and carboxylic groups, respectively.[33] For the Fe_3O_4/GO, the Fe 2p peaks at 711.7 and 725.3 eV are very close to the values of Fe_3O_4.[2] It demonstrates the successful formation of the magnetite nucleus on GO surface. After the coating of PDA, a new N 1s peak was clearly observed at 401 eV. Furthermore, the high resolution XPS spectra of carbon, nitrogen, iron, and oxygen in **Figure 2c-f** gave an obvious evidence for the formation of the PDA polymer layers on the GO surfaces with magnetite Fe_3O_4 nanoparticles.

The Fe_3O_4/GO/PDA 2D-MIPs and NIPs were also characterized by TGA. As shown in **Figure 3a**, a weight loss of approximately 25% was observed for pure GO at 200 °C owning to the evaporation of adsorbed water and the decomposition of labile oxygen.[30] In contrast, a significantly low weight loss of approximately 7% was observed for the Fe_3O_4/GO/PDA 2D-MIPs at 200 °C. However, more weight loss in comparison to GO was observed at a high temperature 700 °C, which confirms the formation of the PDA layer in 2D-MIPs. The 2D-NIPs showed the similar weight loss with 2D-MIPs. Form the XRD patterns of Fe_3O_4–GO and Fe_3O_4/GO/PDA 2D-MIPs in **Figure 3b**, the presence of crystal planes with cubic crystal structures

proves that the 2D-MIPs materials are surely containing crystalline Fe_3O_4.

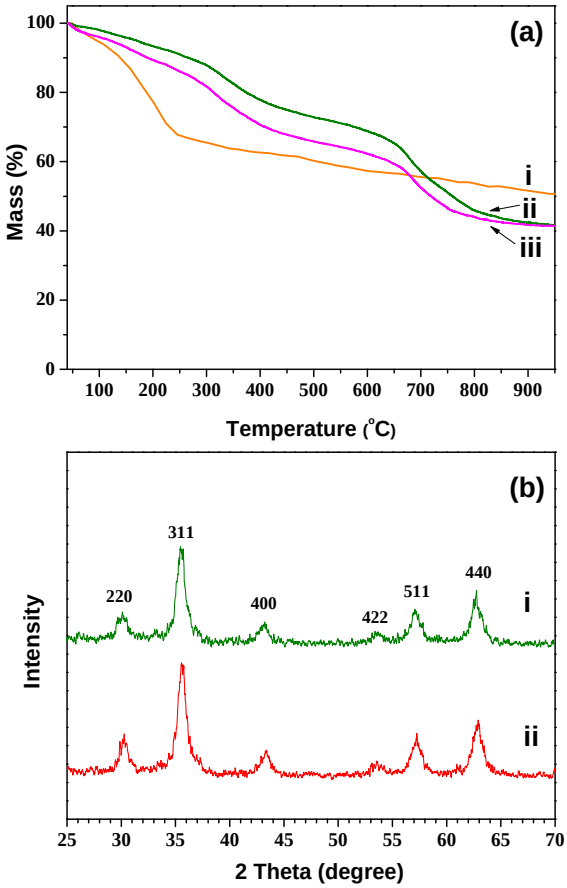

Figure 3 TGA curves (a) of GO (i), Fe_3O_4/GO/PDA 2D-MIPs (ii) and Fe_3O_4/GO/PDA 2D-NIPs (iii), XRD patterns (b) of Fe_3O_4/GO/PDA 2D-MIPs (i) and Fe_3O_4-GO (ii).

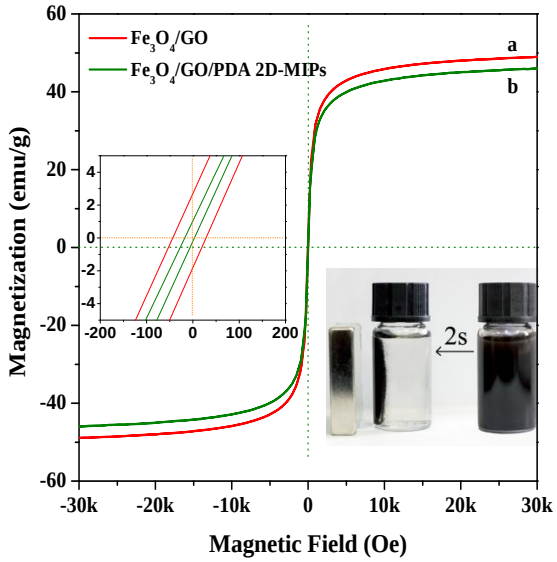

Figure 4 Magnetic hysteresis loops ofFe_3O_4-GO (a) and Fe_3O_4/GO/PDA 2D-MIPs (b) and the magnetic response of Fe_3O_4/GO/PDA 2D-MIPs to external magnetic field.

Since magnetism is a key factor to the rapid separation of proteins, the magnetic property of Fe_3O_4/GO/PDA-MIPs was measured. As presented in **Figure 4**, the saturation magnetization of the Fe_3O_4–GO and Fe_3O_4/GO/PDA 2D-MIPs was 48.9 emu/g and 45.9 emu/g, respectively. The slight decrease of saturation magnetization was attributed the formation of PDA molecular imprinting layers on Fe_3O_4/GO surfaces. However, the 2D-MIPs still exhibit sufficient magnetism and can be rapidly separated by an external magnetic field in a very short time as shown in Figure 4, which brings the convenience for rapid separation of proteins via magnetic 2D-MIPs as illustrated in **Scheme 2**.

Binding Isotherms of Magnetic 2D-MIPs. Adsorption kinetics of Fe_3O_4/GO/PDA 2D-MIPs is one of the key factors to rapid separation. As shown in **Figure 5**, the adsorption processes were obviously dependent on time, and the 2D-MIPs exhibited a fast adsorption rate. The adsorption capacity rapidly increased and reached equilibrium after 10 min. The template proteins could be easily removed or adsorbed from the PDA layers of 2D-MIPs in a short time. From the adsorption kinetics of NIPs, the binding amount is decreased as the increase of adsorption time, demonstrating the high selectivity of the imprinted layer.

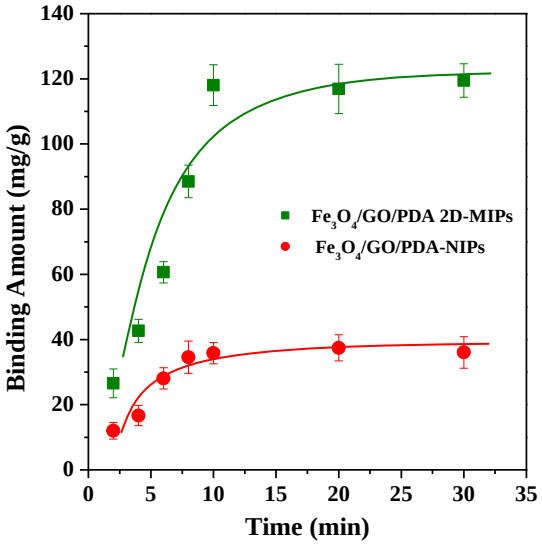

Figure 5 Dynamic rebinding curves of BSA on Fe_3O_4/GO/PDA 2D-MIPs (■) and Fe_3O_4/GO/PDA NIPs (●).

The adsorption capacity of 2D-MIPs or NIPs for BSA was studied by static equilibrium experiments. As shown in **Figure 6a**, the binding amounts of BSA on 2D-MIPs or NIPs are increased as the increase of initial BAS solution concentration (0.4–2.5 mg/mL). It is note that the binding capacity of Fe_3O_4/GO/PDA 2D-MIPs was significantly higher than that of Fe_3O_4/GO/PDA-NIPs, which demonstrate a high specific binding ability of 2D-MIPs for the BSA template proteins. The binding amount of BSA will achieve near saturation at a BSA concentration of 1.5 mg/mL. The maximum adsorption capacity of Fe_3O_4/GO/PDA 2D-MIPs was 117.1 mg/g, which is approximately three times higher than that of Fe_3O_4/GO/PDA-NIPs (37.3 mg/g). Such high binding capacity is attributed to the thin PDA layers on the surfaces of Fe_3O_4/GO, which

ensures a complete removal of the template protein molecules. On the other hand, the high surface-to-volume ratio of 2D Fe_3O_4/GO is helpful to creating more recognition sites in correspondence with the design of 2D-MIPs as discussed in **Scheme 1**.

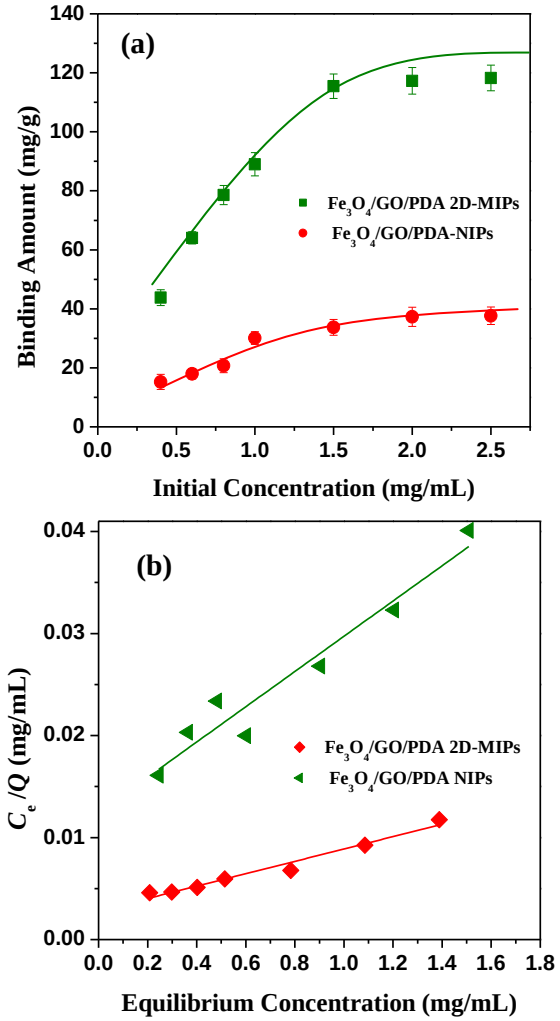

Figure 6 Adsorption isotherm behaviours of BSA (a) on Fe_3O_4/GO/PDA 2D -MIPs (■) and Fe_3O_4/GO/PDA NIPs (●), Langmuir analysis (b) of Fe_3O_4/GO/PDA 2D-MIPs (◆) and Fe_3O_4/GO/PDA NIPs (●).

The data obtained from static absorption experiments were further processed with Langmuir analysis and Freundlich isotherm according to the following equations.[2, 21]

$$C_e / Q = C_e / Q_{\max} + 1/ KQ_{\max} \qquad (3)$$

$$\lg Q = n \lg C_e + \lg K_f \qquad (4)$$

where C_e is the equilibrium concentration of BSA in the supernatant after sorption (mg/mL), Q and Q_{max} is the experimental adsorption capacity (mg/g) of BSA and the theoretical maximum adsorption capacity of the 2D-MIPs materials (mg/g), respectively. The parameter of K is the Langmuir constant related to the energy of adsorption (mL/mg). The Q_{max} and K values can be calculated from the slope and intercept of the linear equation plotted in C_e/Q versus C_e (**Figure 6b)**. The n and K_f are the Freundlich constants, which can be obtained from a linear plot of lg$Q$ versus lgC_e. By comparing the linear correlation coefficients (r), the Langmuir model (r = 0.9846) was observed to be a better fit to the experimental data of BSA on 2D-MIPs than the Freundlich model (r = 0.9058). The Q_{max} and K value calculated from Langmuir model of the Fe_3O_4/GO/PDA 2D-MIPs is 163.9 mg/g and 2.2 mL/mg, respectively. In contrast, the Q_{max} and K value of NIPs were 57.8 mg/g and 1.4 mL/mg, respectively. The results indicated that the Fe_3O_4/GO/PDA-MIPs exhibit a significantly good ability for selectively adsorbing the BSA template proteins.

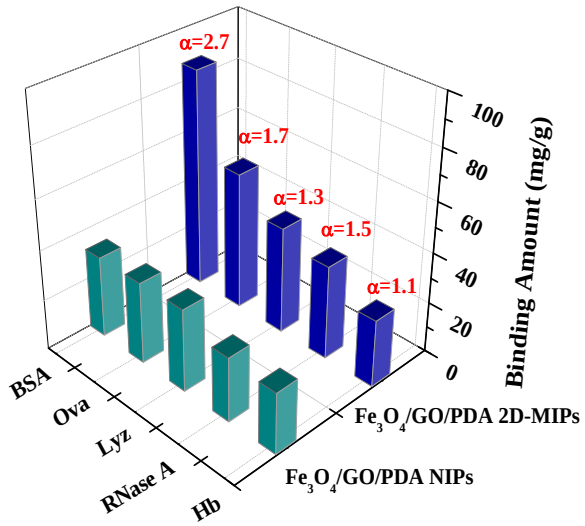

Figure 7 Adsorption amounts of different proteins on Fe_3O_4/GO/PDA 2D-MIPs and Fe_3O_4/GO/PDA NIPs, where the imprinting factors are marked above the bars.

Recognition Specificity of Magnetic 2D-MIPs. To evaluate the selectivity of BSA-Fe_3O_4/GO/PDA 2D-MIPs toward the template proteins of BSA, another four proteins with different isoelectric points (PI) and molecular weight (M_w), including Lyz (14.4kDa, PI=11), Hb (64.5kDa, PI=6.8), Ova (43kDa, PI=4.7), and RNase A (13.7kDa, PI=7.8), were chosen as contrast substrates. **Figure 7** shows the adsorption capacities of the Fe_3O_4/GO/PDA 2D-MIPs or NIPs for different proteins, and the imprinting factor α is calculated according the binding ratio of Fe_3O_4/GO/PDA 2D-MIPs to NIPs.The 2D-MIPs clearly exhibited high selectivity for the template BSA in comparison to other proteins. The α value for BSA of 2.7 is higher than those for the other proteins employed, where the αvalue for binding Lyz, Hb, Ova, and RNase A is 1.3, 1.1, 1.7, and 1.5, respectively. The high adsorption selectivity and specificity of the 2D-MIPs toward the template protein can be attributed to the specific binding sites in the imprinted PDA layer on the 2D surface imparted by imprinting.[21] For the selected proteins, the adsorption of 2D-MIPs was possible because of the noncovalent interaction between proteins and PDA. The amino and hydroxyl groups as well as π-π bonds of PDA can interact with selected proteins in the form of hydrogen bonding and electrostatic interaction.[26] However, the noncovalent interaction was not strong enough to keep the selected proteins staying in the imprinted sites, and the α values of the four

contrast proteins were bigger than 1 but smaller than BSA. The Hb has a size similar to that of the template. However, the Hb is a tetrameric protein composed of pairs of two different polypeptides and is biconcave, while BSA (66 kDa, PI=4.8) is oval and composed of a polypeptide.[34] The different spatial orientation of Hb might limit its access to the binding sites by steric hindrance, thus the adsorption capacity is relatively low. Ova has a PI similar to that of BSA and a smaller size, however, the Ova is easily distributed into the imprinting cavities and exhibits a relatively high adsorption capacity. Moreover, although Lyz and RNase A also have smaller sizes, their PI values are different from that of the template BSA, and the microenvironment with complementarities in shape, size, and function is not suitable for Lyz and RNase A. So the adsorption capacity of Lyz and RNase A is not satisfactory.

Regeneration and Reproducibility of Magnetic 2D-MIPs. The desorption and regeneration are the most important factors for the application of imprinted materials. For this purpose, 10 mg of Fe_3O_4/GO/PDA 2D-MIPs was added to a centrifuge tube containing 5 mL of BSA solution at 1 mg/mL, and the centrifuge tube was subjected to shaking for 10 min at room temperature. The Fe_3O_4/GO/PDA 2D-MIPs were repeatedly washed with an SDS-containing solution (10% w/v) to remove the embedded BSA template molecules.The adsorption–desorption cycles were repeated five times using the same 2D-MIPs **(Figure 8)**. The Fe_3O_4/GO/PDA 2D-MIPs were stable for up to five adsorption cycles only with a marginal decrease of 10.3% in capacity. It is probably attributed to the changing of the recognition cavities in the PDA layers on 2D-MIPs during the repeated washing.

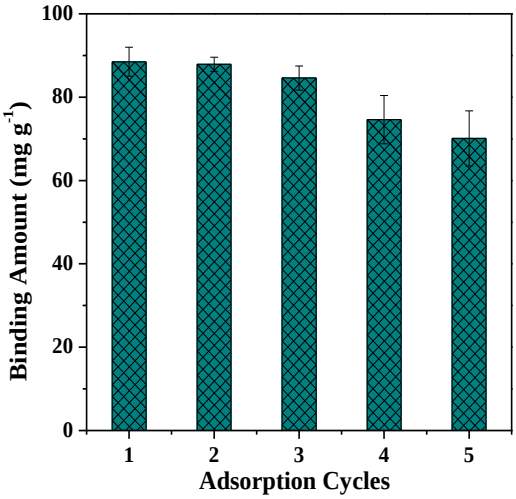

Figure 8 The adsorption–desorption cycles of Fe_3O_4/GO/PDA two-dimensional molecularly imprinted materials.

Real Sample Analysis. The Fe_3O_4/GO/PDA 2D-MIPs were applied in a real bovine blood sample to further evaluate its applicability and separation effectiveness. The samples were analysed using HPLC-UV and the chromatograms of the 200-fold diluted bovine blood solution, extracted by 2D-MIPs and NIPs, and standard BSA concentration of 0.4 mg/mL as shown in **Figure 9**. In contrast, the chromatogram of standard BSA solution was also presented (**Figure 9d)**. It can be observed that the BSA was existed in the blood sample with the matrix interference (**Figure 9a**). The selective separation of BSA from bovine blood sample was obtained in the solutions extracted by 2D-MIPs (**Figure 9b**), and no apparently BSA peak was observed in **Figure 9c** in the solutions extracted by 2D-NIPs. These results demonstrated that the prepared 2D-MIPs can selectively separate BSA in real bovine blood sample, which gives guidance for the separation of targeted protein from complex samples without multistep treatment procedures.

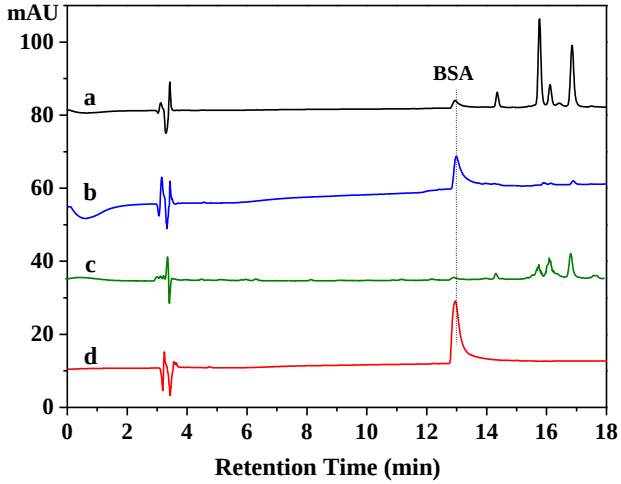

Figure 9 Chromatograms of the 200-fold diluted bovine blood solution (a), the 200-fold diluted bovine blood solution extracted with 2D-MIPs (b), the 200-fold diluted bovine blood solution extracted with 2D-NIPs (c), the BSA standard solution (d).

Conclusions

The magnetic two-dimensional molecularly imprinted materials for highly recognition and separation of proteins were prepared via the bovine serum albumin (BSA)-surface-imprinted PDA on Fe_3O_4–graphene oxide surfaces. The maximum adsorption capacity of 2D-MIPs was 117.1 mg/g, which is approximately three times higher than that of NIPs. The thin PDA layers on the surfaces of 2D Fe_3O_4/GO ensures rapid adsorption and removal of the BSA template protein molecules. The prepared material was easily collected using an external magnetic because of the super paramagnetic behaviour of Fe_3O_4/GO. The binding properties of BSA on magnetic 2D-MIPs and real sample analysis demonstrated high recognition specificity, selectivity, accessibility and convenient separation of proteins. The magnetic 2D-MIPs presented in this work provide a new perspective for the design of surface molecular imprinting materials with potential in recognition and separation of proteins.

Acknowledgements

This work was supported by the National Natural Science Foundation of China (21404085/21174112), China Postdoctoral Science Foundation (2014M552486), Shaanxi Province Postdoctoral Science Foundation and the Fundamental

Research Funds of NPU (GEKY8003). J.K. acknowledges the support from New Century Excellent Talents of the Education Ministry of China (NCET-11-0817).

References

1 X. Xiao, K. Yan, X. Xu and G. Li, *Talanta*, 2015, **138**, 40-45.

2 X. Xie, X. Pan, S. Han and S. Wang, *Anal. Bioanal.Chem.*, 2015, **407**, 1735-1744.

3 X. Xie, F. Wei, L. Chen and S. Wang, *J. Sep. Sci.*, 2015, **38**, 1046-1052.

4 C. C. Hong, P. H. Chang, C. C. Lin and C. L. Hong, *Biosens. Bioelectro.*, 2010, **25**, 2058-2064.

5 X. T. Shen, C. G. Xu, K. M. A. Uddin, P. O. Larsson and L. Ye, *J. Mater. Chem. B*, 2013, **1**, 4612-4618.

6 C. Algieri, E. Drioli, L. Guzzo and L. Donato, *Sensors*, 2014, **14**, 13863-13912.

7 M. Esfandyari-Manesh, M. Javanbakht, R. Dinarvand and F. Atyabi, *J. Mater. Sci. Mater.-M.*, 2012, **23**, 963-972.

8 T. Zhou, L. Jorgensen, M. A. Mattebjerg, I. S. Chronakis and L. Ye, *Rsc Adv.*, 2014, **4**, 30292-30299.

9 R. Gao, Y. Hao, S. Zhao, L. Zhang, X. Cui, D. Liu, Y. Tang and Y. Zheng, *Rsc Adv.*, 2014, **4**, 56798-56808.

10 G. Zhu, J. Fan, Y. Gao, X. Gao and J. Wang, *Talanta*, 2011, **84**, 1124-1132.

11 X. J. Li, B. L. Zhang, L. Tian, W. Li, H. P. Zhang and Q. Y. Zhang, *Senso. Actuat. B-Chem.*, 2015, **208**, 559-568.

12 M. E. Corman, C. Armutcu, L. Uzun, R. Say and A. Denizli, *Colloid Surf. B*, 2014, **123**, 831-837.

13 H. Chen, J. Kong, D. Yuan and G. Fu, *Biosens. Bioelectro.*, 2014, **53**, 5-11.

14 D.-Y. Li, X.-W. He, Y. Chen, W.-Y. Li and Y.-K. Zhang, *ACS Appl. Mater. Interfaces*, 2013, **5**, 12609-12616.

15 J. Bognar, J. Szucs, Z. Dorko, V. Horvath and R. E. Gyurcsanyi, *Adv. Funct. Mater.*, 2013, **23**, 4703-4709.

16 X. Wang, Q. Kang, D. Shen, Z. Zhang, J. Li and L. Chen, *Talanta*, 2014, **124**, 7-13.

17 A. Nematollahzadeh, A. Shojaei, M. J. Abdekhodaie and B. Sellergren, *J. Colloid Interface Sci.*, 2013, **404**, 117-126.

18 Z. Zhang, X. Yang, X. Chen, M. Zhang, L. Luo, M. Peng and S. Yao, *Anal. Bioanal.Chem.*, 2011, **401**, 2855-2863.

19 R. Gao, X. Mu, Y. Hao, L. Zhang, J. Zhang and Y. Tang, *J. Mater. Chem. B*, 2014, **2**, 1733-1741.

20 K. S. Novoselov, A. K. Geim, S. V. Morozov, D. Jiang, Y. Zhang, S. V. Dubonos, I. V. Grigorieva and A. A. Firsov, *Science*, 2004, **306**, 666-669.

21 J. Luo, S. Jiang and X. Liu, *J. Phys. Chem. C*, 2013, **117**, 18448-18456.

22 L. Shang, F. Zhao and B. Zeng, *ACS Appl. Mater. Interfaces*, 2014, **6**, 18721-18727.

23 S. Han, X. Li, Y. Wang and S. Chen, *Rsc Adv.*, 2015, **5**, 2129-2136.

24 S. D. Pan, H. Y. Shen, L. X. Zhou, X. H. Chen, Y. G. Zhao, M. Q. Cai and M. C. Jin, *J. Mater. Chem. A*, 2014, **2**, 15345-15356.

25 H. Lee, S. M. Dellatore, W. M. Miller and P. B. Messersmith, *Science*, 2007, **318**, 426-430.

26 Z. Xia, Z. Lin, Y. Xiao, L. Wang, J. Zheng, H. Yang and G. Chen, *Biosens. Bioelectro.*,2013, **47**, 120-126.

27 T. Chen, M. Shao, H. Xu, S. Zhuo, S. Liu and S.-T. Lee, *J. Mater. Chem.*, 2012, **22**, 3990-3996.

28 M. Zhang, X. Zhang, X. He, L. Chen and Y. Zhang, *Nanoscale*, 2012, **4**, 3141-3147.

29 S. D.Pan, H. Y.Shen, L. X.Zhou, X. H.Chen, Y. G.Zhao, M. Q.Cai and M. C.Jin, J. Mater. Chem. A 2014, **2**, 15345-15356.

30 W. S. Hummers and R. E. Offeman, *J. Am. Chem. Soc.*, 1958, **80**, 1339-1339.

31 W. F. Zhao, Y. S. Tang, J. Xi and J. Kong, *Appl. Surf. Sci.*, 2015, **326**, 276–284

32 T. Tran Viet and A. Sandhu, *Mater. Sci. Eng. B-Adv.*, 2014, **189**, 13-20.

33 J. Kong, M.J. Wang, J.H. Zou and L.N. An, *ACS Appl. Mater. Interfaces*, 2015, **7**, 6733–6744.

34 Y.-Q. Xia, T.-Y. Guo, H.-L. Zhao, M.-D. Song, B.-H. Zhang and B.-L. Zhang, *J. Biomed. Mater. Res. A*, 2009, **90A**, 326-332.